A density rise experiment on PLT

To cite this article: J.D. Strachan *et al* 1982 *Nucl. Fusion* **22** 1145

A DENSITY RISE EXPERIMENT ON PLT

J.D. STRACHAN, N. BRETZ, E. MAZZUCATO, C.W. BARNES*,
D. BOYD**, S.A. COHEN, J. HOVEY, R. KAITA, S.S. MEDLEY,
G. SCHMIDT, G. TAIT, D. VOSS†
Princeton University,
Plasma Physics Laboratory,
Princeton, New Jersey,
United States of America

ABSTRACT. The evolution of the density profile in PLT during intense gas puffing is documented and analysed. Measurements of the spectrum of low-energy edge neutrals and of the change in central neutral density indicate that charge-exchange processes alone cannot account for the central density rise. The transient density profile changes can be reproduced numerically by a diffusivity of $\sim 10^4\ cm^2 \cdot s^{-1}$ and a spatially averaged inward flow of $10^3\ cm \cdot s^{-1}$. These transport coefficients are $10-10^2$ times larger than neoclassical. The ion energy confinement is reduced, the small-scale density fluctuations are increased, and runaway electron losses are increased during the density rise.

INTRODUCTION

Plasma densities have been raised by gas puffing in a number of tokamak experiments [1–6]. In the smaller devices, the evolution of the density profile can be explained by assuming an edge-neutral temperature of 10–50 eV. This allows edge neutrals to penetrate deeply into the plasma before being ionized. However, for larger devices such as PLT, or at the higher densities found in Alcator, the mean free path for edge-neutral penetration becomes much smaller than the minor radius. Nevertheless, in PLT and Alcator the electron density profiles have remained parabolic, as was observed in the smaller devices. Previously, the density rise was modelled [6, 7] with neoclassical transport modified by an increased edge-neutral energy caused, for example, by neutral interactions at the limiter, and by a modestly enhanced (2–3 times) Ware pinch. Such small deviations from neoclassical transport cannot explain the rapid changes in density reported here.

Gas can be puffed rapidly into PLT, doubling the density in 50–100 ms, but causing only small deviations from parabolic density profiles. However, because of the short mean free path, charge exchange cannot be an important transport process in the interior of PLT. In fact, without an anomalous transport mechanism, the edge density will rise rapidly, further shielding the centre from edge neutrals. Therefore, experimental determination of the rate of central density increase and of the resulting density profiles indicates a deviation from neoclassical transport. It is this deviation and its consequences which are described in this article.

The approach in this work has been primarily empirical. It was found that the central density rise comes from the puffing gas, and not from a pinching of the initial plasma particles. A charge-exchange mechanism can be excluded, since the central neutral density does not change during gas puffing. The outflux of low-energy neutral particles was measured near to and away from the limiter. Although the increase in recycling near the limiter is considerable, no increase is observed in the outflux of higher-energy (300–1000 eV) edge neutrals at either location. These observations limit the models that can be used to explain the particle balance. If a simple one-dimensional transport model is assumed [8–10], the observation of parabolic density profiles implies that the density rise is due to both an inward flow velocity, which is about $10^3\ cm \cdot s^{-1}$ near the edge, decreasing to $\sim 10^2\ cm \cdot s^{-1}$ near the centre, and a diffusion coefficient of $\sim 10^4\ cm^2 \cdot s^{-1}$. These values are 10 to 10^2 times larger than neoclassical and for the flow velocity the radial

* Present address: Los Alamos National Laboratory, Los Alamos, New Mexico, USA.
** Department of Physics and Astronomy, Maryland Univ., College Park, USA.
† Present address: California Univ., Livermore, Lawrence Livermore Lab., USA.

dependence is opposite to that of the Ware pinch. However, in order to make the ion energy balance consistent with the inferred particle flows, either the ion heat conduction must be enhanced six to seven times during the density rise or the inward transport has to involve primarily colder particles.

To help identify possible mechanisms responsible for the transport, spatially resolved measurements of the density fluctuation spectrum have been made with 2 mm microwaves. During the rise, the magnitude of the fluctuations is observed to increase substantially.

When the density rises, the ion confinement time decreases. However, despite the anomalies in the particle balance, both the electron and the ion confinement following the density rise increase and become comparable to the highest PLT values.

EXPERIMENT

Unless otherwise noted, the PLT device [11] was operated with top-bottom carbon limiters, a = 40 cm, R = 135 cm, B = 25 kOe, I = 400 kA, and titanium-gettered walls. The physical locations of the relevant diagnostics are shown in Fig. 1. The gas injection valve is near the limiter. Its injection rate is controlled by a feedback system in which the difference between the measured line average density and its programmed evolution determines the voltage on a piezoelectric valve [12]. The response of the total system including the gas valve conductance is $\lesssim 5$ ms.

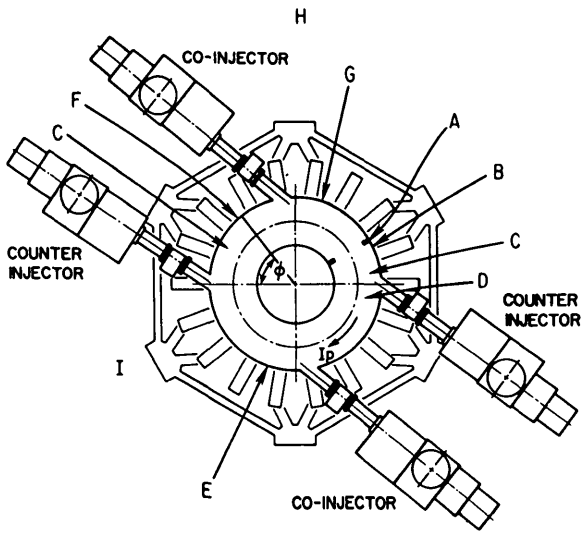

FIG. 1. Schematic diagram of PLT, indicating the toroidal location of the relevant diagnostics and equipment: A – limiters; B – gas inlet, $2\omega_{ce}$ polychrometer; C – charge-exchange diagnostic; D – microwave scattering; E – Thomson scattering; F – low-energy neutral analyser, movable limiter; G – bolometer; H – hard X-ray detector; I – neutron detectors.

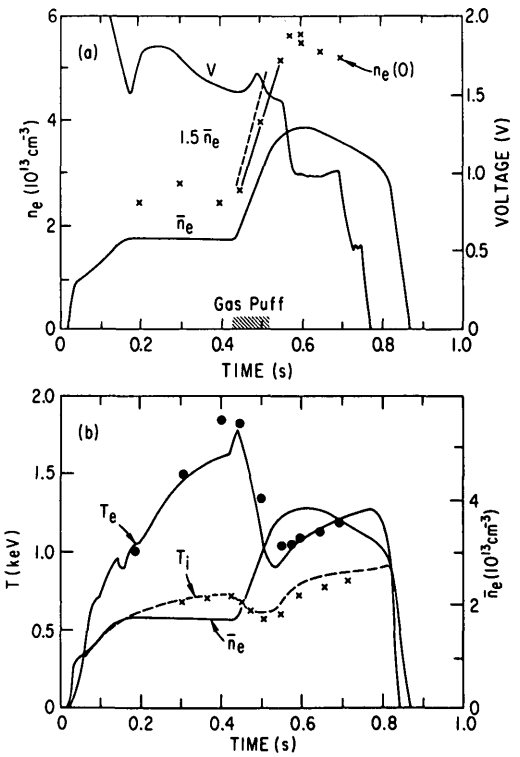

FIG. 2. (a) Time evolution of the loop voltage, V, the line-average density $\bar{n}_e$, and the central electron density, $n_e(0)$ during the density rise. (b) Time evolution of the central electron temperature from $2\omega_{ce}$ (——), and from TVTS (●), with the time evolution of the central ion temperature from neutrons (- -), and from charge exchange (X) during the density rise.

The density was increased from $\bar{n}_e \cong 2 \times 10^{13}$ cm^{-3} to 4×10^{13} cm^{-3} in about 100 ms (Fig. 2(a)). The density profile determined from Thomson scattering remained centrally peaked during gas puffing (Fig. 3(a), (c)). The density profiles have a systematic asymmetry caused by a slight misalignment between the Thomson scattering laser and the spectrometer [13]. The data shown in Fig. 3(c) are uncorrected for this and the 3-D plot averages the profiles about the centre. The central density is delayed with respect to the line-averaged density value ($1.5 \times \bar{n}_e$) by 10–20 ms. The density evolution is reproducible, as are the current and voltage waveforms. However, there are occasional changes in the MHD activity in the equilibrium before the density rise. Before the rise, sawtooth oscillations are often not observed, but during and after the rise they almost always occur.

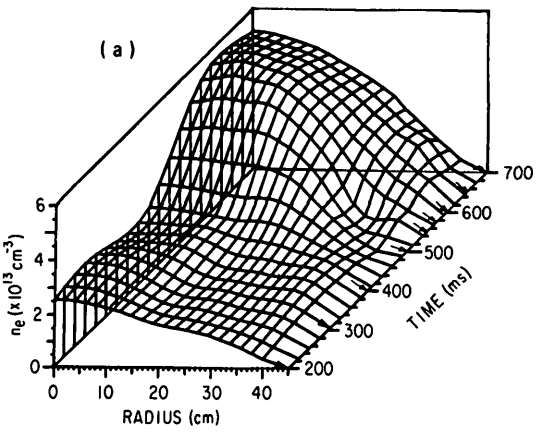

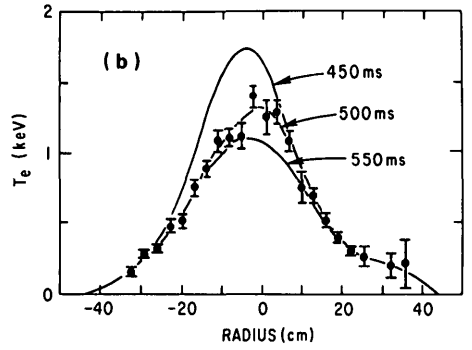

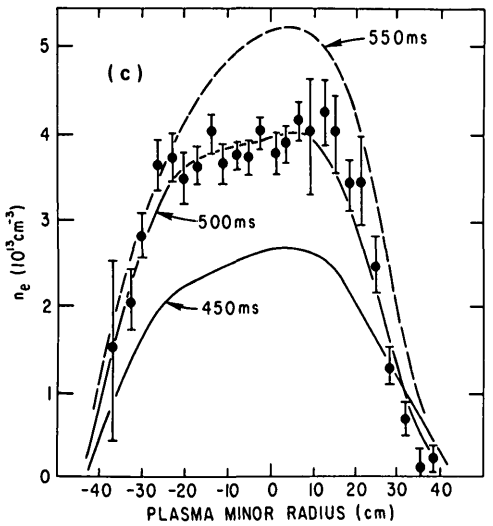

FIG. 3. (a) Evolution of the density profile as determined by Thomson scattering; (b) $T_e(r)$ profiles at selected times in the density rise; (c) $n_e(r)$ profiles at selected times in the density rise.

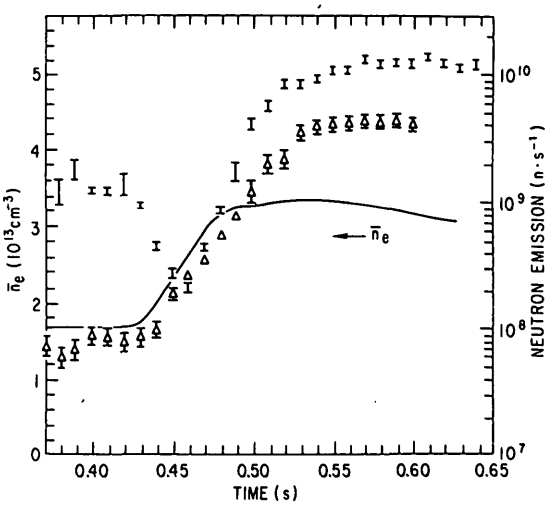

FIG. 4. Time evolution of the neutron emission during a deuterium gas puff into a deuterium plasma (I) and into a hydrogen plasma (Δ).

When the initial plasma and the puffing gas are both deuterium, the neutron emission falls during the density rise (Fig. 4) but rises afterwards to a level which is ten times higher. The ion temperature deduced from the charge-exchange spectrum and from neutron emission falls by about 100 eV during the rise but returns thereafter to its initial level (Fig. 2(b)).

The plasma current rises at a small rate throughout the discharge (0.2 kA·ms^{-1}). The loop voltage rises somewhat during the density rise and thereafter falls to about 1 volt per turn. The peak electron temperature is shown in Fig. 2(b) from the $2\omega_{ce}$ emission. The increase in T_e just before the density rise occurs at the beginning of the sawtooth MHD activity. Some differences between the emission and Thomson scattering measurements may be due to the fact that the emission resolution is about 10 cm vertical and about 3 cm horizontal, while the Thomson scattering profiles [13] are measured along a vertical chord at R = 134 cm, with a vertical resolution of 3 cm and a horizontal resolution of 3 mm. The profiles of Fig. 3 were made up of 24 Thomson scattering profiles measured at ten times during the discharges and thus form a multiple shot composite of the plasma evolution.

The role of impurities in the power balance is relatively small. The total radiated power profile measured by the bolometer array (Fig. 1) is relatively flat. The central value is ~30 mW·cm^{-3}, rising to ~50 mW·cm^{-3} between 30 and 40 cm. Thus, the radiated loss in the central region is ⩽10% of the

Ohmic power input of 400–500 mW·cm^{-3} and the radiated power equals the Ohmic input only in the outer regions ($r \geqslant 30$ cm). The influence of the density rise is to temporarily increase the edge radiation by ~30%. The initial plasma has $Z_{eff} \cong 1.5$–2 from resistivity measurement, and $Z_{eff} = 2.0$–3.0 from spectroscopy. After the density increase, Z_{eff} drops to 1.0 (resistivity) to 1.5 (spectroscopy). Thus, the influx of gas does not bring in new impurities. The edge radiations from CIII, H_β and similar lines do increase by factors of 3–20 during the gas puff; however, immediately after the rise in density, the line intensities revert back to their previous levels [6, 14]. A more complete account of the spectroscopic measurements in this type of discharge can be found in Ref. [12].

The data shown in Figs 2 and 3 refer to an initial deuterium plasma with a deuterium gas puff. In order to determine the rate at which the puffing gas arrives in the centre, two similar auxiliary experiments have been carried out. Hydrogen has been puffed into a deuterium plasma and deuterium into a hydrogen plasma. The evolution of the measured parameters is nearly identical to that described for puffing deuterium into a deuterium plasma. The neutron emission for pure deuterium and for deuterium puffed into an initial hydrogen plasma is shown in Fig. 4. The expected centrally peaked profile of the ion temperature ensures that all the neutrons come from $r/a \leqslant 1/4$; thus, the ion temperature dependence can be unfolded from the emission rate, yielding the time evolution of the central deuteron density. The result for puffing deuterium into a hydrogen plasma is shown in Fig. 5. The central density rise can be entirely accounted for by particles puffed from the gas valve, since the increase in neutron emission can be accounted for by the deuterium reaching the plasma centre. Also, when hydrogen is puffed into an initially deuterium discharge, the neutron emission remains nearly constant. The central deuteron density (Fig. 6) also remains relatively constant, indicating that there is no substantial change in the amount of initial plasma gas recycled at the plasma edge and, as in the previous case, no large expulsion or concentration of the original discharge gas during the density rise.

The uncertainty in the central ion temperature evolution makes these determinations somewhat uncertain, since the neutron emission depends roughly on $n_e^2 T_i^4$. It should be noted from Fig. 4 that deuterium puffing into a hydrogen plasma immediately caused the neutron emission to rise, in spite of the falling ion temperature. This implies that immediate penetration

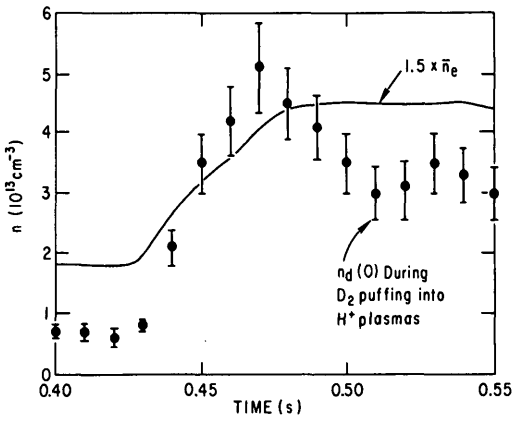

FIG. 5. Central deuteron density during a deuterium gas puff into a hydrogen plasma. The error bars arise from counting statistics.

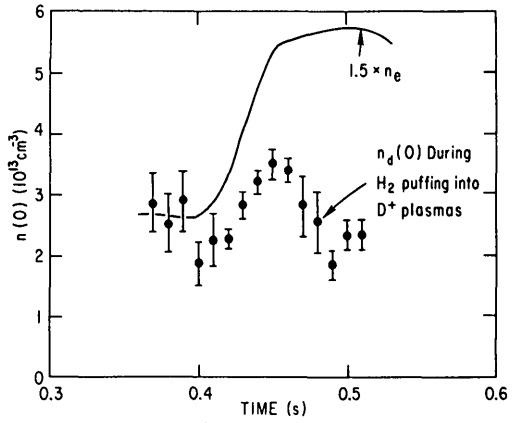

FIG. 6. Central deuteron density during a hydrogen gas puff into a deuterium plasma. The error bars arise from counting statistics.

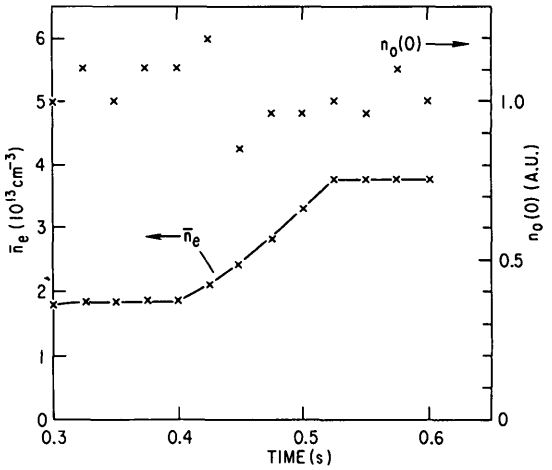

FIG. 7. Relative time evolution of the central neutral density at a toroidal location near the limiter and gas inlet, as determined by the charge-exchange emission.

of the puffing gas due to a transport process must be taking place, since multiple charge exchange would not allow penetration of the injected gas.

The evolution of the central neutral density has been deduced from the energetic charge-exchange outflux at two toroidal locations. The magnitude of the neutral outflux is corrected for the time evolution of the ion temperature and the fractional escape of the neutrals out of the plasma. Well away from the limiter ($\sim 110°$ toroidally – see Fig. 1), the central neutral density falls by a factor of two, but near the gas inlet ($\sim 10°$ toroidally – see Fig. 1) and limiter ($\sim 15°$), the central neutral density remains relatively constant (Fig. 7) during the rise. We conclude from these measurements that the rise in central density cannot be accounted for by ionization of neutrals at the centre.

The outflux of low-energy (50–1000 eV) neutrals from the periphery of the discharge has been measured by a time-of-flight spectrometer [15] and by depth implantation of deuterium in carbon probes [16] (Fig. 1). Away from the limiter and gas valve, the outflux of neutrals with energies of $\gtrsim 50$ eV decreases during the gas puff by a factor of two and the average energy decreases by 30%. The outflux near the limiter is simulated at this toroidal location by inserting an auxiliary carbon button limiter from the top of the vessel at the neutral spectrometer port (Fig. 1). This limiter was adjusted to receive about 20% of the power deposited on the main limiter. With the button limiter inserted, the average neutral flux was 10–50 times higher and the time evolution during the gas puff was relatively constant. The lower-energy flux increased (Fig. 8(a)), while the higher-energy flux (Fig. 8(b)) decreased. The shape of the low-energy spectrum reveals that the edge-ion temperature decreases from 45 (± 10) eV to 20 (± 10) eV.

The absolute magnitude and shape of the measured neutral outflux spectrum was used to estimate the absolute values of the edge and central neutral densities at the limiter. The estimate is based upon a calculation of the expected neutral emission [15] using the measured values of $T_e(r)$, $n_e(r)$, $T_i(0)$, and the edge-neutral temperature as variable parameters. Before gas puffing (300 ms in Fig. 8), the edge-neutral density is $n_0(a) \sim 2 \times 10^9$ cm^{-3} and the central neutral density is $n_0(0) \cong 1 \times 10^8$ cm^{-3}; at the end of gas puffing (475 ms) these values are: $n_0(a) \cong 7 \times 10^9$ cm^{-3} and $n_0(0) \cong 5 \times 10^7$ cm^{-3}. The values of n_0 away from the main limiter and the auxiliary limiter are estimated to be about seven times lower. The uncertainties in these values, due to the absolute calibration and the plasma opacity, are about a factor of two.

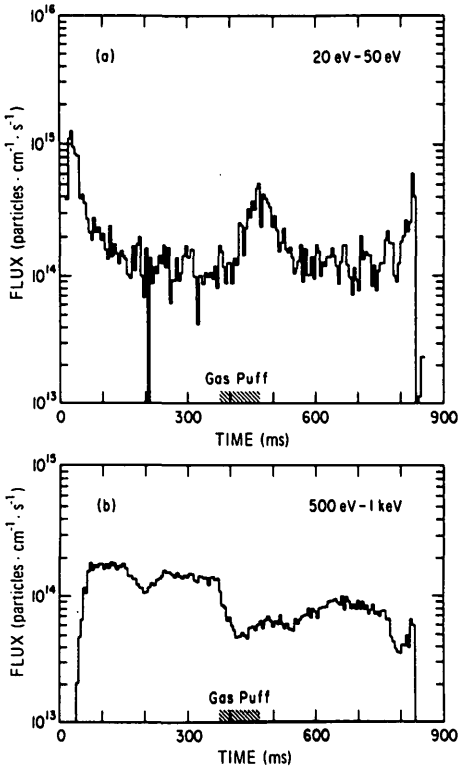

FIG. 8. (a) Neutral outflux at the movable limiter in the energy range 20–50 eV during an intense gas puff. (b) Neutral outflux at the movable limiter in the energy range 500 eV–1 keV during an intense gas puff.

The neutral particle data imply that the energetic deuterium source function at the edge of the plasma does not change substantially when the density increases owing to the gas puff. Furthermore, the decrease in higher-energy flux allows less neutral particle penetration through the plasma boundary. As a result, it can be expected that the density increase must be explained ultimately by plasma transport processes.

ENERGY CONFINEMENT TIME

The central electron power balance ($r \leqslant 15$ cm) is shown in Fig. 9. The input power from Ohmic heating is balanced primarily by electron conduction before the density rise; afterwards, 25–50% of the input is lost to the ions. The uncertainty in the central power input is due to an uncertainty in the current

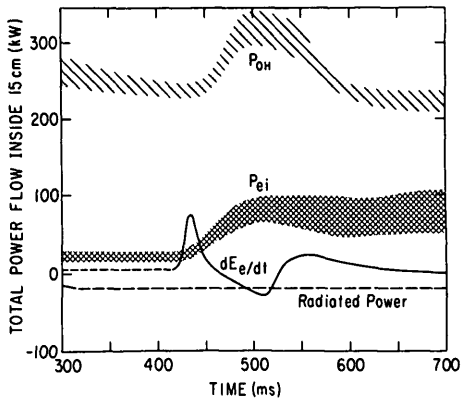

FIG. 9. Central electron power flow ($r \leqslant 15$ cm) for the discharges of Figs 2 and 3. P_{OH} is the Ohmic power input, P_{ei} is the electron ion coupling.

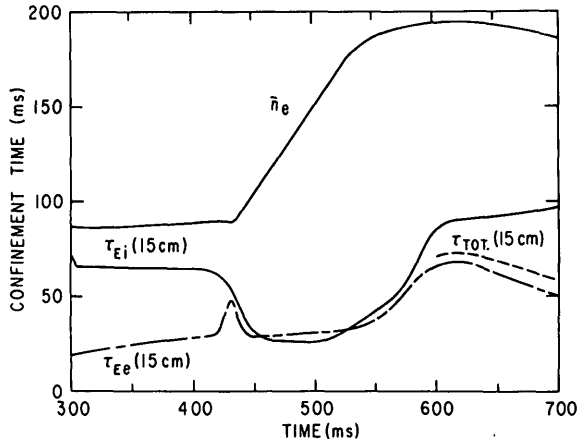

FIG. 10. Empirical electron and ion energy confinement times in the central plasma region ($r \leqslant 15$ cm).

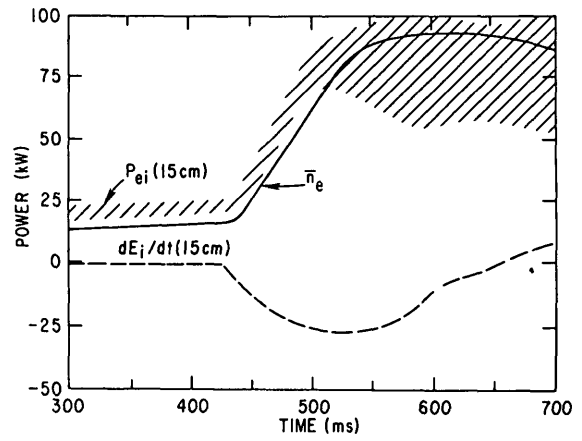

FIG. 11. Central ion power flow ($r \leqslant 15$ cm) for the discharges of Figs 2 and 3.

distribution. During the density rise, the profile changes are rapid enough that it is necessary to calculate the internal fields using the magnetic diffusion equation:

$$\frac{\partial}{\partial r}\left[\frac{\eta}{r}\frac{\partial (rB_\theta)}{\partial r}\right] - \mu_0 \frac{\partial B_\theta}{\partial t} = 0 \qquad (1)$$

The resistivity, η, is a function of the measured electron temperature and (more weakly) of B_θ through the trapped-particle correction. The current and loop voltage are used to calculate $Z_{eff}(t)$ self-consistently from the temperature measurements. If the radial profile of Z is assumed constant, $q(0) \cong 0.7$ after the density rise. A central accumulation of impurities, or the absence of any trapped-particle correction to the resistivity, can raise the estimate of q(0) to 0.9–1.0. However, the central power input is uncertain only to about 20% because a lower current density is roughly compensated by an increased resistivity. Usually, q(0) is thought to be ~1.0, especially with sawtooth MHD activity present.

The central electron energy confinement time, τ_{Ee}, can be calculated from the time evolution of the electron energy content, E_e:

$$\tau_{Ee}\ (15\ \text{cm}, t) = \frac{\int_0^{15\text{cm}} E_e r dr}{\int_0^{15\text{cm}} (P_{OH} - P_{ei} - dE_e/dt) r dr} \qquad (2)$$

The initial value of τ_{Ee} shown in Fig. 10 is about 35 ms, which is typical of PLT confinement times at this density [17]. The electron confinement time remains relatively constant throughout the density rise but increases to 60 ms at the density maximum, primarily because the loop voltage falls and the power transferred to the ions goes up, leaving less power to be lost through the electron channel.

The ion energy content triples as a result of the density rise. The empirical ion energy flow (Fig. 11) indicates that an increase occurs in the power input from electron/ion collisions (P_{ei}). If the measurement uncertainties in both T_e and T_i are taken into account, the error in P_{ei} after the rise is considerable. However, we take the upper boundary of the P_{ei} estimate to obtain the lower bound on the ion energy confinement time, τ_{Ei}, for $r \leqslant 15$ cm, as shown in Fig. 10

$$\tau_{Ei}\ (15\ \text{cm},t) = \frac{\int_0^{15\text{cm}} E_i r dr}{\int_0^{15\text{cm}} (P_{ei} - dE_i/dt) r dr} \qquad (3)$$

The ion confinement time begins at about 60 ms, decreases during the gas puff as P_{ei} increases, but rises back to its previous level after the density increase has stopped.

The total energy confinement time

$$\tau_E = \frac{\int_0^a (E_e + E_i)\ r dr}{\int_0^a \left[P_{OH} - \frac{d}{dt}(E_e + E_i)\right] r dr} \qquad (4)$$

is dominated by the electrons but rises to 80–90 ms at 600–650 ms in the discharge (Fig. 12). This value is close to the highest one attained in PLT [14].

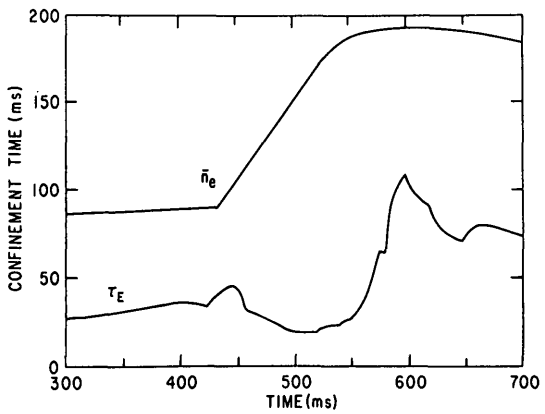

FIG. 12. Total energy confinement time for the discharges of Figs 2 and 3.

PARTICLE BALANCE

The electron density ($n_e = n_i = n$) is presumed to change in time, owing to diffusion by either neoclassical (D^{NC}) or anomalous (D^A) processes, directed convection by either neoclassical (Ware drifts, V^W) or anomalous (V^A) processes, and ionization of neutrals by electron impact ionization ($\langle\sigma v\rangle_{ei}$)

$$\frac{\partial n}{\partial t} = \frac{1}{r}\frac{\partial}{\partial r}\left[r(D^{NC} + D^A)\ \frac{\partial n}{\partial r}\right]$$

$$+ \frac{1}{r}\frac{\partial}{\partial r}\left[rn(V^W + V^A)\right] + nn_o\langle\sigma v\rangle_{ei} \qquad (5)$$

The neoclassical coefficients for the Ware pinch velocity (Fig. 13(a)) and the diffusion coefficient [7]

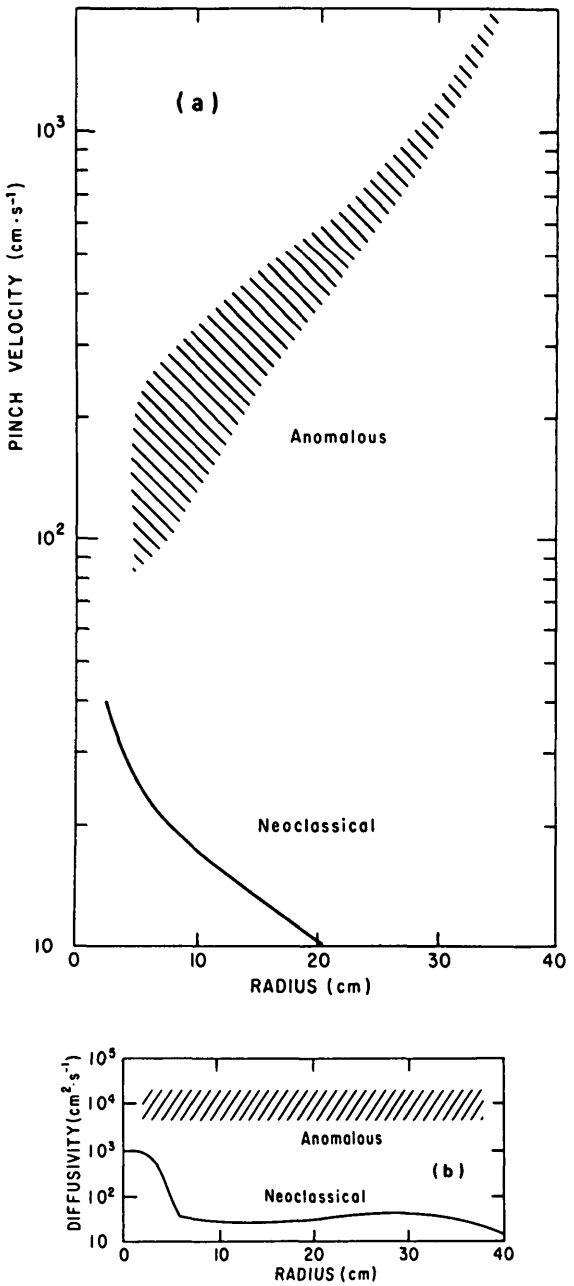

FIG. 13. (a) Neoclassical and anomalous pinch velocities used in particle balance; (b) Neoclassical and anomalous diffusion coefficients used in particle balance.

(Fig. 13(b)) have rather small numerical values for PLT [6]. Neoclassical theory is unable to describe the experimental density rise. Thus the experimental evolution of the plasma density profile is used to obtain information on the anomalous coefficients. The calculation of the neutral density profile is uncertain since the edge-neutral density and temperature are difficult to determine experimentally.

The one-dimensional diffusion equation (Eq. (5)) was solved by the Crank-Nicholson implicit difference method. The spatial diffusion was averaged in time. The edge-neutral density and edge-neutral temperature are considered input variables. The consequence of a purely neoclassical calculation for the experimental PLT parameters is that the density profile becomes hollow (Fig. 14), contrary to the experimental observations. Increasing the neutral penetration by changing the edge-neutral energy to 500 eV during the gas puff still results in a hollow density profile. The basic problem is that the neutral gas penetration is unstable to the hollowing of the density profile (i.e. building up the edge density) during intense gas puffing. Once the edge density begins to flatten, there is less neutral penetration, resulting in a faster build-up of edge density, and so on. Another way of expressing this problem is that the combined action of the neoclassical inward velocity and the neoclassical diffusion coefficient is insufficient to transport particles away from the edge region where they build up because of ionization of the neutrals whose density has been increased by gas puffing. A comparison of the neoclassical terms contributing to the change in particle density is shown in Fig. 15.

An arbitrary increase (X 10) in the pinch velocity, keeping the diffusion neoclassical, can increase the central density at the experimentally observed rate (Fig. 16). However, the density profile becomes more peaked inside r = 15 cm than is observed, and the ten times neoclassical pinch cannot prevent the profile from hollowing at the edge.

Pure neoclassical calculations are unable to account for the experimentally observed density rise in PLT, even with a five to ten times enhanced edge neutral temperature and/or a ten times enhanced Ware pinch. At the minimum, the transport processes nearer the plasma periphery (r > 25 cm) need to be enhanced over neoclassical. The anomalous diffusion coefficient and anomalous inward-directed velocity in Eq. (5) are used to estimate the magnitude of the anomalous transport processes. If the anomalous processes dominate the entire particle balance, then the typical steady-state parabolic density profiles provide a

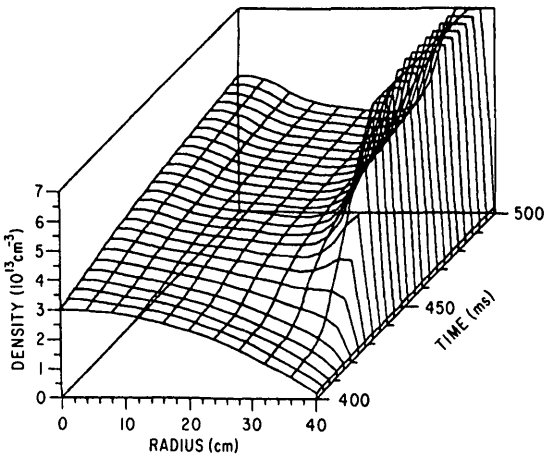

FIG. 14. Evolution of the density profile, starting from an initial parabolic profile and evolving through a gas puff, for the case of neoclassical transport coefficients.

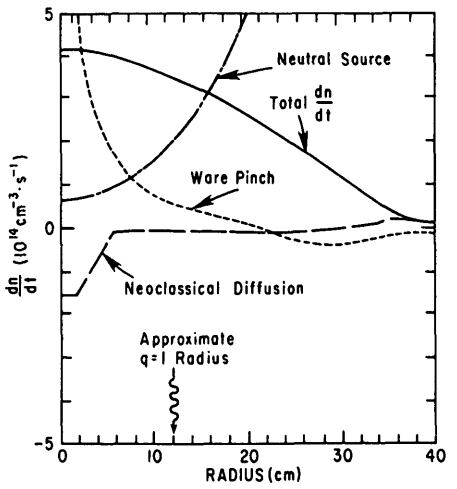

FIG. 15. Magnitude of the rate of density change caused by the neoclassical transport coefficients.

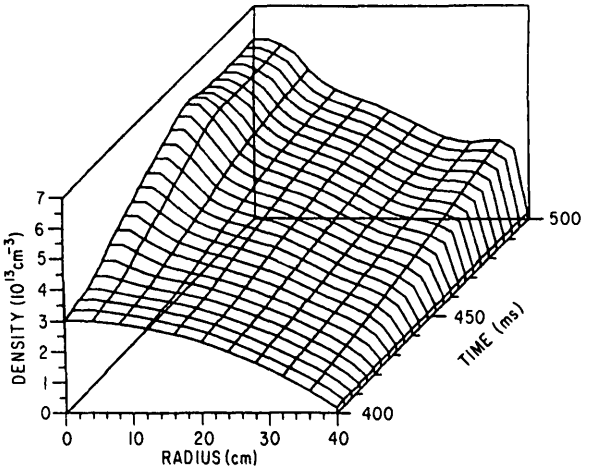

FIG. 16. Evolution of the density profile, starting from an initial parabolic profile and evolving through a tenfold enhancement of the Ware pinch, without an increase in the edge-neutral density.

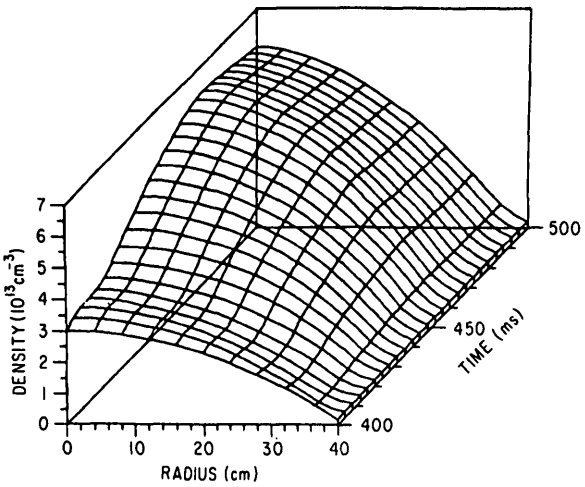

FIG. 17. Evolution of the density profile, starting from an initial parabolic profile and evolving through a gas puff, using the anomalous transport coefficients of Fig. 13.

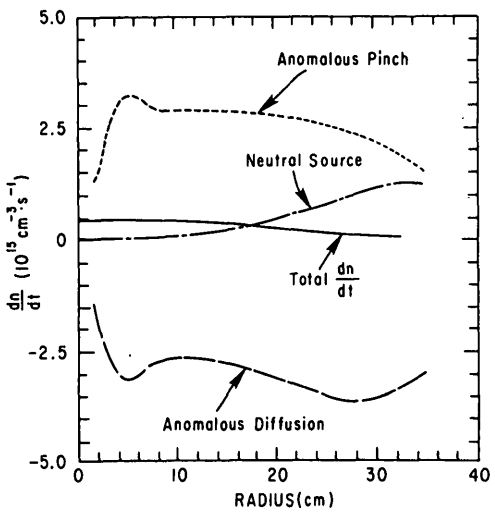

FIG. 18. Magnitude of the rate of density change caused by the anomalous transport coefficients.

specific relationship between the anomalous inward-directed velocity and the anomalous diffusion [8]

$$v^A(r) = -\frac{2rD^A}{a^2-r^2} = \frac{D^A}{n}\frac{\partial n}{\partial r}\Big|_{\text{parabolic n profiles}} \quad (6)$$

Following Coppi [8], the steady-state plasma convection is modelled as a competition between a radially independent diffusion process (Fig. 13(b)) and an inward-directed velocity (Fig. 13(a)); this competition is larger toward the plasma periphery such that the two processes balance when the profile is parabolic. This means that a slight flattening of the density will allow the inward velocity term to dominate over the diffusion, tending to restore the parabolic profile.

Calculations with this type of anomalous process indicate that a diffusion coefficient of about 10^4 cm$^2\cdot$s^{-1} (to within a factor of about three) is required to explain the PLT gas puffing experiments. Most of the density increase is due to the anomalous inward velocity, while the large diffusion coefficient is required for a quick relaxation back to a near-parabolic profile (Fig. 17). The anomalous contributions to the change in density are shown in Fig. 18.

It is also difficult to explain the PLT results using calculations with only a large anomalous diffusion coefficient that is independent of r and no large inward-directed velocity. The equilibrium profiles themselves tend to be flat and the density tends to become hollow during the density rise.

ION ENERGY BALANCE

Since the particle balance is anomalous, with inward and outward fluxes exceeding the net particle flux by a factor of about ten, it is interesting to examine the neoclassical ion energy balance for the discharges in Figs 2 and 3. The ion energy flow (dE_i/dt) is balanced according to

$$\frac{dE_i}{dt} = P_{ei} + P_{tc} + P_{pc} + P_{cx} - P_{iz} \quad (7)$$

for which the electron ion coupling (P_{ei}), the neoclassical thermal conduction (P_{tc}), the charge-exchange losses (P_{cx}) and the re-ionization energy gain (P_{iz}) are defined in Ref. [18].

The particle convection term, P_{pc}, is defined by

$$P_{pc} = \frac{1}{r}\frac{\partial}{\partial r}\left[r\,\frac{3}{2}\,kT_i\Gamma\right] + \frac{nkT_i}{r}\frac{\partial}{\partial r}(r\,\Gamma/n) \quad (8)$$

where the net particle flux, Γ, is used, which is determined through the particle balance equation

$$\frac{\partial n}{\partial t} = \frac{1}{r}\frac{\partial}{\partial r}(r\Gamma) + nn_o\langle\sigma v\rangle_{ei} \quad (9)$$

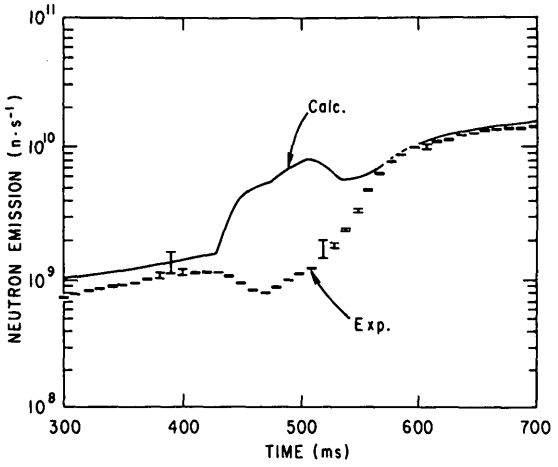

FIG. 19. Time evolution of the neutron emission (I) for the discharges of Figs 2 and 3. The solid line is the calculated neutron emission on the basis of the neoclassical ion energy balance.

The ion temperature evolution is modelled by assuming a steady state at 300 ms and taking experimental values for $T_e(r, t)$, $n_e(r, t)$ and Z_{eff}. The value $q(0, t) = 1.0$ was arbitrarily fixed during the rise and $B_\theta(r, t)$ determined by assuming the current profile to be proportional to $T_e^{3/2}$. The results discussed here are relatively insensitive to the form of $q(r)$. Relative to the diffusion calculation discussed earlier, the neoclassical heat conduction coefficient [18] ($\propto q^2$) may be slightly overestimated for $r \lesssim 10$ cm and slightly underestimated for the outer portion of the discharge. We have also initially taken a toroidally averaged value of $n_0(r = 0) \cong 10^8$ cm^{-3}. Any value larger than this would be inconsistent with the initial ion energy balance and is somewhat higher (five times) than is expected from the low-energy neutral data. The profiles of n_0 and T_0 are calculated from a short mean-free-path model of Ref. [19]. The time evolution of $n_0(r = 0)$ is taken from the experimental data.

The calculation shows that before and after the density rise the heat loss can be explained mainly by neoclassical heat conduction to the boundary. However, during the rise, the inward flow of heat from convection and electron/ion coupling is not balanced by neoclassical conduction and, as a result, the model predicts an increase in the ion temperature instead of the observed decrease. Figure 19 shows the predicted neutron flux, compared with the experimental value. The calculation can be made to agree with the experiment in several possible ways:

(a) The heat conduction can be increased during the density rise by a factor of 6–7
(b) The central neutral particle density can be increased by a factor of ~10 (in contradiction to our charge-exchange measurements which show the central density to be constant or decreasing)
(c) The net particle influx brings little energy into the plasma centre, i.e. the anomalous convection process brings particles into the centre but little energy, as if the convection were an energy-dependent process.

Of these possibilities, (b) can be excluded by the measurements and particle-balance modelling, but so far we cannot distinguish between (a) and (c), each of which is possible.

FLUCTUATIONS

The small-scale electron density fluctuations measured in PLT by scattering of microwaves [20, 21] were observed to change during the rapid rise of the plasma density. An array of antennae, located in the same poloidal plane, was used for launching the output of an extended interaction oscillator of 140 GHz and for collecting the waves scattered by fluctuations of the plasma density. Spatial resolution was obtained by using high-gain antennae (≅38 db). The typical scattering region had a length of about 10 cm in the radial direction. The k-resolution ($\cong \pm 1$ cm^{-1}) was determined by the finite dimensions of the scattering volumes.

The differential cross-section for incoherent scattering of electromagnetic waves by electron density fluctuations is

$$\sigma = \sigma_0 S(\bar{k}, \omega)$$

where $\sigma_0 = (e^2/mc^2)^2$ is the Thomson cross-section and $S(\bar{k}, \omega)$ is the spectral density of electron fluctuations. The frequency ω and the wave vector $\bar{k}$ must satisfy the energy and momentum conservation, i.e. $\omega = \omega_s - \omega_i$ and $\bar{k} = \bar{k}_s - \bar{k}_i$, where the subscripts s and i refer to the scattered wave and the incident wave, respectively.

Shown in the insert in Fig. 20 is the typical frequency spectrum of fluctuations, with $k \cong 7$ cm^{-1}, during the stationary phase of a discharge, with $\bar{n}_e = 1.3 \times 10^{13}$cm^{-3}.

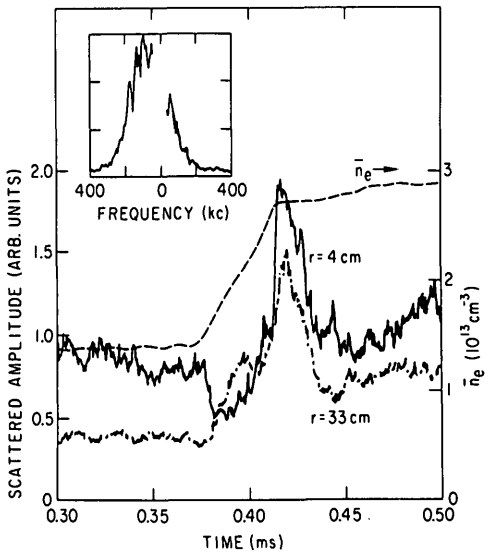

FIG. 20. Time evolution of the microwave signal scattered from small-scale density fluctuations in the outer and central plasma regions. The insert shows a typical scattered spectrum which extends to 200 kHz.

The spectrum is shifted towards the negative frequency side which, for this particular scattering geometry, is that of waves with phase velocities along the electron diamagnetic velocity. From these measurements we estimate that the quantity $\langle \ln^2 \rangle / \langle n \rangle$ has a value of $\cong (0.5-1.0) \times 10^{-2}$ in the central region of the discharge ($r \cong 0 - 15$ cm) and a value of $\cong (2-4) \times 10^{-2}$ in the outer region ($r \cong 30-40$ cm).

The time evolution of density fluctuations at two radial locations is shown in Fig. 20 for a discharge where the average density was raised from 1.4×10^{13} cm^{-3} to 2.8×10^{13} cm^{-3} in about 40 ms. Figure 20 shows the quantity

$$\left[\int_{-\infty}^{+\infty} S(k, \omega) d\omega \right]^{1/2}$$

From these data, one can see that at the edge of the plasma column the fluctuation level starts to increase as soon as the density begins to rise and reaches a maximum after 20 ms. At the same time, in the central region of the plasma column, the turbulence at first decreases to a minimum and then returns to its original value. At this moment, the fluctuation amplitude starts to increase rapidly throughout the plasma column and reaches a maximum at the end of the density rise. The ratio of the peak over the initial amplitude is about a factor of two in the central region and four in the outer region. The peak amplitude increases with the rate of density rise. The spectral shift in the electron diamagnetic direction tends to increase in the outer region and to diminish in the centre during the density rise.

As the plasma density stops rising, the turbulence decreases to a new stationary level which, with respect to the amplitude before the density rise, is almost unchanged in the central region while it is about two times larger (or equal to the ratio of the density increase) in the outer region.

There is also a similarity between the time evolution of the density fluctuations and that of hard X-ray emission caused by runaway electrons leaving the plasma and striking the limiter. On other PLT discharges [22] the fluctuation spectrum of the hard X-ray signal was similar to the spectrum of the density fluctuations. During the density rise, the time evolution of both signals is similar (Fig. 21), as is the time evolution of the low-energy neutral outflux (Fig. 8(a)). The peak of the hard X-ray signal also increases with the rate of density rise. For the discharges used in the density rise experiments, the runaway electron levels were too low to obtain meaningful fluctuation spectra.

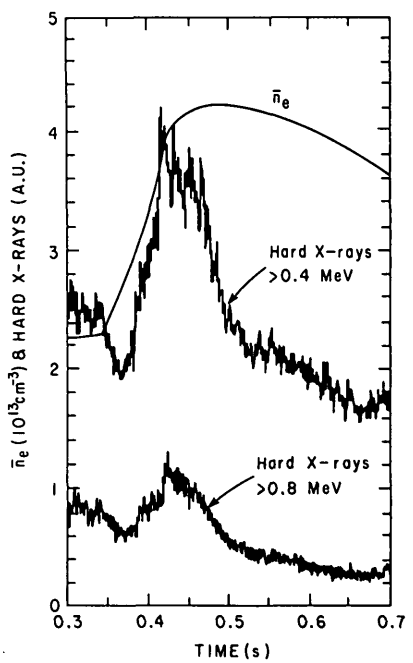

FIG. 21. Time evolution of the hard X-ray emission caused by runaway electron bombardment of the limiter.

INCREASED RATE OF DENSITY RISE

When the rate of density rise is increased beyond that described in the previous section, the magnitude of the density fluctuations increases (Fig. 22), the dip in the neutron intensity (and thus T_i) is enhanced, the density profile flattens, and the loop voltage increases (to 1.9 V for $dn/dt \cong 7 \times 10^{14}\ cm^{-3} \cdot s^{-1}$). The discharges tend to become irreproducible and disruptive when the rate of density rise is above $\dot{\bar{n}}_e \cong 5 \times 10^{14}\ cm^{-3} \cdot s^{-1}$. The tendency toward disruptions is reduced if neutral beam heating is used during the density rise. Figure 23 shows a beam-assisted density rise, where the electron density is increased from $\bar{n}_e \cong 1.6 \times 10^{13}\ cm^{-3}$ to $\bar{n}_e \cong 6 \times 10^{13}\ cm^{-3}$, with $dn/dt \cong 2 \times 10^{15}\ cm^{-3} \cdot s^{-1}$. Deuterium beams of 1.8 MW are used to maintain the plasma temperature at $T_e(0) \cong 1.3$ keV, $T_i(0) \cong 2.0$ keV. The initial plasma is deuterium, the puffing gas is helium in order to aid the neutral beam penetration, the toroidal field is 32 kG, and $I_\phi \cong 450$ kA. The gas puffing is intense enough to form a hollow density profile with the maximum at r = 20–30 cm. The beam itself makes no appreciable contribution to the density rise, either at the density maximum or at the plasma centre (less than 10% is caused by beam particles).

One expectation is that the main influence of neutral beam heating is to stabilize the electron temperature and current density profiles, which would otherwise undergo considerable redistribution because of the large influx of cold gas. These beam-assisted density rises provide further empirical evidence for the magnitude of the particle transport coefficients. The hollow density profile means that it is feasible for the central density to rise entirely by a diffusive process. Putting

$$\frac{\partial n}{\partial t}\ (r = 0) \cong D^A \frac{1}{r} \frac{\partial}{\partial r}\ (r \frac{\partial n}{\partial r})$$

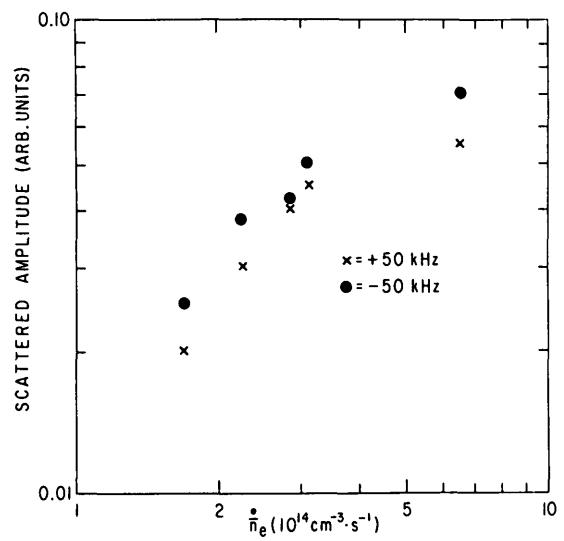

FIG. 22. Amplitude of the peak in the scattered microwave signal as a function of the rate of density rise.

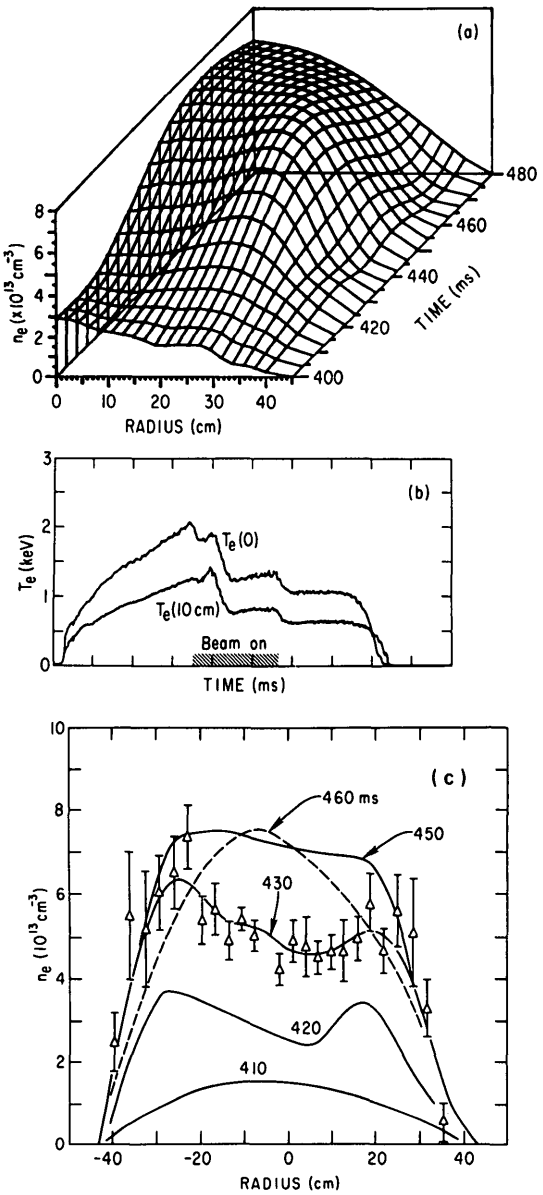

FIG. 23. (a) Time evolution of the density profile as determined by Thomson scattering for a strong beam-assisted density rise; (b) Time evolution of the central electron temperature; (c) $n_e(r)$ profiles at selected times in the beam-assisted density rise.

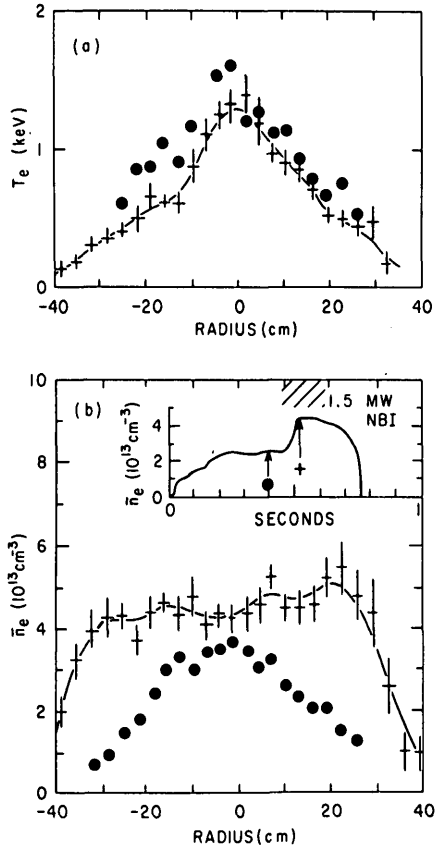

FIG. 24. Temperature and density profiles for a beam-assisted density rise.

means that D^A is of the order of 5×10^3 cm$^2 \cdot$s^{-1} for it to account for the experimentally observed $\partial n/\partial t \sim 2 \times 10^{15}$ cm$^{-3} \cdot$s^{-1}, with the experimentally observed $\partial n/\partial r \sim 10^{12}$ cm^{-2}. The anomalous coefficients (Fig. 13) used earlier can also reproduce the experimentally observed profiles (Fig. 23) where now the diffusive term (D^A) dominates the directed velocity term (V^A) due to the inverted profile.

Another case of beam-assisted density rise provides further empirical evidence for the magnitude of the directed velocity term (V^A) (Fig. 24). Now, $\dot{\bar{n}}_e \sim 10^{15}$ cm$^{-3} \cdot$s^{-1} was obtained with 1.5 MW of deuterium beam heating of a hydrogen plasma, and the density profile was flat throughout the steepest part of the density rise (Fig. 24). In this case $\partial n/\partial r \cong 0$, so that diffusive terms (even if D is a function of minor radius) are less important. Putting

$$\frac{\partial n}{\partial t}\ (r = 0) \simeq \frac{1}{r}\frac{\partial}{\partial r}\, rnV^A$$

means that a spatially averaged velocity V^A is of the order of 10^3 cm$\cdot$s^{-1}. Again, modelling this density rise with both anomalous coefficients (Fig. 13) reproduces the experimentally observed profiles, and the directed velocity term does dominate inside $r \sim 30$ cm.

The fact that the density profiles do not change appreciably until the rate of density rise becomes $\sim 10^{15}$ cm$^{-3} \cdot$s^{-1} and only become hollow for $\dot{\bar{n}}_e \sim 2 \times 10^{15}$ cm$^{-3} \cdot$s^{-1}, empirically indicates that the particle influx rate is larger than the outflux due to transport. For the lower rates of density rise (Figs 2 and 3), $\dot{\bar{n}}_e \cong 2 \times 10^{14}$ cm$^{-3} \cdot$s^{-1}, the profiles were not highly perturbed, since the transport processes were much larger than the particle influx rate (Fig. 18).

DISCUSSION

The evolution of the density profile during gas puffing experiments on PLT indicates that particle transport could be due to the combination of an inwardly directed velocity ($V^A \sim 10^3$ cm$\cdot$s^{-1}) that is peaked towards the plasma periphery, and a large anomalous diffusion coefficient ($D^A \sim 10^4$ cm$^2 \cdot$s^{-1}), as has been suggested previously on the basis of Alcator gas puffing experiments [8]. This experimental conclusion is derived from PLT plasma conditions where the density rises strongly and the plasma is evolving in time. However, these transport coefficients for the hydrogen ions would also explain PLT transport measurements of trace high-Z impurities [23] and trace ^{3}He ions [24] which were performed in quasi-steady-state plasma conditions. The results reported here cannot be explained by enhanced neutral penetration, coupled with a mildly enhanced Ware pinch, which has previously been used to explain PLT and Alcator density profiles [7]. The enhanced Ware pinch leads to more peaked profiles rather than slightly broader profiles. Enhanced neutral penetration, as might be caused by an increased edge neutral temperature, leads to hollow density profiles. Charge-exchange measurements of the central neutral density evolution and the neutral emission from the limiter indicate that neutral particle penetration did not cause the density rise. Since an inwardly directed velocity is necessary to model the experimental results, it is worth considering possible mechanisms for the generation of this inward drift.

The results reported here do not directly contradict an inwardly directed velocity produced by modes driven by the electron temperature gradient [25], $v \propto (\partial T_e/\partial r)$, but earlier PLT results with hollow

electron temperature profiles had centrally peaked density profiles instead of the hollow density profiles expected when the pinch was driven by electron temperature gradients [26].

The pinch velocity (Fig. 13) has roughly the same radial profile as the neutral density, since both terms fall by one to two orders of magnitude from the plasma periphery to the plasma centre. The pinch velocity is $\sim 10\rho_i/\tau_{cx} \sim \rho_\theta/\tau_{cx}$ when averaged over the plasma, and is $\sim\rho_i/\tau_{cx}$ near the limiter and gas inlet, where ρ is the Larmour radius and τ_{cx} is the charge-exchange time. Thus, mechanisms are possible which involve ion displacement by the charge-exchange process. Also, it is expected that the cold gas will perturb the plasma column in the vicinity of the gas inlet and the limiter. This perturbation should have a radial profile similar to the neutral density profile; thus, mechanisms are possible which involve electric fields set up by three-dimensional asymmetries.

There may be a connection between the inward flow and microturbulence. The pinch velocity (Fig. 13) has roughly the same radial profile as the density fluctuations in PLT [27] since both fall by one to two orders of magnitude from the plasma periphery to the plasma centre. Moreover, the density rise and density profile evolution have a major influence on the magnitude of the density fluctuations. The pinch velocity of 10^3 cm·s^{-1}, with $\delta n/n$ of a few per cent, requires a specific phase relationship between poloidal electric and density perturbations such that the cosine of the phase is $\sim 0.1-1$. Recent experiments on Macrotor [28] found potential and density fluctuations to be correlated, but the phase was not specified. The decrease of scattered amplitude at the end of the density rise is consistent with the observed improvement in energy confinement (Fig. 10).

Finally, we note that the evolution of the ion energy balance during the density rise indicates that, whereas the usual neoclassical analysis applies during the quasi-steady portions of the discharge, an anomaly exists during the density rise. The anomaly might be explained by a five times enhanced ion thermal conduction or an energy-dependent convection process that brings little energy into the plasma centre. There is a fundamental difficulty with the usual treatment of the convection term in the ion energy balance, since the inward and outward fluxes are much larger than the net flux of particles that is conventionally used to deduce the convective energy flow. This means that, if there is any energy dependence, more energy can be transported by the inward or outward convection processes. We note that differences in energy confinement between different tokamaks, and in heating quality between different experiments, may originate with the convection processes since such differences are often accompanied by density profile changes [12, 29] and particle recycling changes.

ACKNOWLEDGEMENTS

The authors thank W. Stodiek, J. Hosea and the PLT experimental group, as well as H. Eubank and the PLT neutral beam group for their help in performing these experiments. Helpful discussions with A. Boozer and W. Tang are also gratefully acknowledged. This work was supported by the United States Department of Energy Contract No. DE-AC02-76-CH03073.

REFERENCES

[1] HOSEA, J.C., BOBELDIJK, C., GROVE, D.J., in Plasma Physics and Controlled Nuclear Fusion Research 1971 (Proc. 4th Int. Conf. Madison, 1971) Vol. 2, IAEA, Vienna (1971) 425.

[2] KLÜBER, O., ENGLEHARDT, W., CANNICI, B., GERNHARDT, J., GLOCK, E., KARGER, F., LISITANO, G., MAYER, H.M., MIESEL, D., MORANDI, P., SESNIC, S., STADLBAUER, J., WAGNER, F., Nucl. Fusion 15 (1975) 1194.

[3] TOI, K., ITOH, S., KADOTA, K., KAWAHATA, K., NODA, N., SAKURAI, K., SATO, K., TANAHASHI, S., XASUE, S., Nucl. Fusion 19 (1979) 1643.

[4] APGAR, E., COPPI, B., GONDHALEKAR, A., HELAVA, H., KOMM, D., MARTIN, F., MONTGOMERY, B., PAPPAS, D., PARKER, R., OVERSKEI, D., in Plasma Physics and Controlled Nuclear Fusion Research 1976 (Proc. 6th Int. Conf. Berchtesgaden, 1976) Vol. 1, IAEA, Vienna (1977) 247.

[5] BUZANKIN, V.V., VERSHKOV, V.A., DNESTROVSKIJ, Yu.N., IZVOZCHIKOV, A.B., MIKHAJLOV, E.A., PEREVERZEV, G.V., in Plasma Physics and Controlled Nuclear Fusion Research 1978 (Proc. 7th Int. Conf. Innsbruck, 1978) Vol. 1, IAEA, Vienna (1979) 287.

[6] SCHMIDT, G.L., BRETZ, N.L., HAWRYLUK, R.J., HOSEA, J.C., JOHNSON, D.W., in Proc. 1st Fusion Funding Workshop, U.S. DOE, Washington, DC (1978) 53.

[7] HUGHES, M.H., Princeton Univ., Plasma Physics Lab., Rep. PPPL-1411 (1978).

[8] COPPI, B., Comments Plasma Phys. Controll. Fus. 5 (1980) 261.

[9] COPPI, B., SHARKY, N., Nucl. Fusion 21 (1981) 1363.

[10] BEHRINGER, K., ENGELHARDT, W., FUSSMANN, G., and the ASDEX Team, in Divertors and Impurity Control (Proc. IAEA Tech. Committee Meeting Garching, 1981), Max-Planck-Institut für Plasmaphysik, Garching (1981) 42.

[11] GROVE, D., ARUNASALAM, V., BOL, K., BOYD, D., BRETZ, N., et al., in Plasma Physics and Controlled Nuclear Fusion Research 1976 (Proc. 6th Int. Conf. Berchtesgaden, 1976) Vol. 1, IAEA, Vienna (1977) 21.
[12] HINNOV, E., HOSEA, J., HSUAN, H., JOBES, F., MESERVEY, E., SCHMIDT, G., SUCKEWER, S., Nucl. Fusion 22 (1982) 325.
[13] BRETZ, N., DIMOCK, D., FOOTE, V., LANG, D., TOLNAS, E., Appl. Opt. 17 (1978) 192.
[14] HAWRYLUK, R., BOL, K., BRETZ, N., DIMOCK, D., EAMES, D., et al., Nucl. Fusion 19 (1979) 1307.
[15] VOSS, D.E., COHEN, S.A., J. Vac. Sci. Technol. 17 (1980) 303.
[16] COHEN, S.A., DYLLA, H.F., WAMPLER, W.R., MAGEE, C.W., J. Nucl. Mater. 93 & 94 (1980) 109.
[17] BOL, K., ARUNASALAM, V., BITTER, M., BOYD, D., BRAU, K., et al., in Plasma Physics and Controlled Nuclear Fusion Research 1978 (Proc. 7th Int. Conf. Innsbruck, 1978) Vol. 1, IAEA, Vienna (1979) 11.
[18] BRUSATI, M., DAVIS, S.L., HOSEA, J.C., STRACHAN, J.D., SUCKEWER, S., Nucl. Fusion 18 (1978) 1205.
[19] GOLDSTON, R.J., Princeton Univ., Plasma Physics Lab., Rep. PPPL-1443 (1978).
[20] MAZZUCATO, E., Phys. Fluids 21 (1978) 1063.
[21] MAZZUCATO, E., Princeton Univ., Plasma Physics Lab., Rep. PPPL-1653 (1980).
[22] BARNES, C.W., DEWAR, R.L., MAZZUCATO, E., STRACHAN, J.D., Phys. Lett. A 81 (1981) 275.
[23] STODIEK, W., GOLDSTON, R., SAUTHOFF, N., ARUNASALAM, V., BARNES, C., et al., in Plasma Physics and Controlled Nuclear Fusion Research 1980 (Proc. 8th Int. Conf. Brussels, 1980) Vol. 1, IAEA, Vienna (1981) 9.
[24] CHRIEN, R., EUBANK, H.P., MEADE, D.N., STRACHAN, J.D., Nucl. Fusion 21 (1981) 1661.
[25] ANTONSEN, T., COPPI, B., ENGLADE, R., Nucl. Fusion 19 (1979) 641.
COPPI, B., SPIGHT, C., Phys. Rev. Lett. 41 (1978) 551.
[26] BOOZER, A., Private communication.
[27] MAZZUCATO, E., Phys. Rev. Lett. 48 (1982) 1828.
[28] ZWEBEN, S., TAYLOR, R.J., Nucl. Fusion 21 (1981) 193.
[29] GOLDSTON, R., DAVIS, S., EUBANK, H., HAWRYLUK, R., JOHNSON, D., et al., Heating in Toroidal Plasmas (Proc. 2nd Joint Varenna – Grenoble Int. Symp. Como, 1980).

(Manuscript received 8 April 1982)